ISSN 0915-633X

NATIONAL INSTITUTE FOR FUSION SCIENCE

Bootstrap Current in the Large Helical Device with Unbalanced Helical Coil Currents

K. Ichiguchi, N. Nakajima, M. Okamoto

(Received - Mar. 17, 1997)

NIFS-492 Apr. 1997

RESEARCH REPORT
NIFS Series

NAGOYA, JAPAN

Bootstrap Current in the Large Helical Device with Unbalanced Helical Coil Currents

Katsuji Ichiguchi, Noriyoshi Nakajima, Masao Okamoto

National Institute for Fusion Science,

Nagoya 464-01, Japan

Abstract

The Large Helical Device (LHD), which is a Heliotron/Torsatron device with two helical coils, is designed so that the current in each helical coil can be controlled independently. Unbalancing these currents leads to spatial axis configurations. It is reported here that the bootstrap current is strongly affected by the imbalance of these currents. When the ratio of the currents in the two helical coils is small enough, the bootstrap current flows in a direction so as to decrease the rotational transform because of the enhancement of the bumpiness component of the magnetic field as well as the spatial axis component. This leads to improved stability.

Key Words ;

bootstrap current, Large Helical Device(LHD), spatial axis, Heliotron/Torsatron, MHD, Mercier stability, unbalanced helical coil currents.

1 Introduction

The Large Helical Device (LHD)[1, 2], which is under construction at Toki in Japan, is a stellarator of the Heliotron/Torsatron variety. This, 3.9 meter major radius, device consists of two helical coils with 10 field periods, and three pairs of poloidal field coils. This design allows many different magnetic configurations. The so-called standard configuration is optimized from the point of view of high beta plasma. good confinement of high-energy particles and diverter action. In this case, the magnetic axis is planar and is located at 3.75m from the major axis and the cross section, averaged in the toroidal direction, is almost circular.

In most previous magneto-hydrodynamic (MHD) studies for Heliotron/Torsatron plasmas, currentless equilibria were investigated. However, it is well known from neoclassical transport theory that, for finite beta, the bootstrap current can effect a net toroidal current [3, 4]. Watanabe et al.[5, 6] developed a method to obtain self-consistent bootstrap currents in Heliotron/Torsatron configurations for three-dimensional (3D) equilibria by iterating the 3D equilibrium calculation performed by the VMEC code[7] and a calculation of the net toroidal current based on neoclassical theory. They found that substantial bootstrap currents flow in the LHD standard configuration. The direction of the bootstrap current flow was such as to increase the rotational transform at the plasma surface.

The effect of such net toroidal currents on Mercier stability [9, 10] was studied by Ichiguchi et al.[8]. They showed that stability depends strongly on the direction of the net toroidal current. A current which increases the rotational transform from that of the zero net current case, has a destabilizing contribution and vice versa. Thus, it would seem that it is important, for LHD stability, to find a configuration in which the bootstrap current will decrease the rotational transform from that of the zero net current case. To do this the bootstrap current must flow in the opposite direction from which it flows in the standard configuration. Watanabe et al.[5] found that by changing the dipole and the quadrupole components of the magnetic field, they could only reduce the bootstrap current but could not reverse its direction. On the other hand, Shaing et al.[11] found that the the bootstrap current in the ATF Torsatron can reverse directions when the currents in

the helical coils are unbalanced and the plasma is in the $1/\nu$ regime. They showed that the reversal of the bootstrap current is attributed to the spatial (non-planar) axis which is created by the $\ell = 1$ helical field, where ℓ denotes the pole number of the helical coils.

LHD also has the ability to achieve spatial axis configurations by unbalancing the currents flowing in the helical coils. Matsumoto et al.[12] studied such configurations but they limited their study to the case of zero net current. They found that the dominant effect on MHD stability was due to changes in the aspect ratio caused by the unbalanced helical currents. In the studies presented here, we obtain substantial changes in some of the MHD properties due to the spatial axis geometry in the presence of the bootstrap current. And, indeed, we find that stability can be achieved by having the net bootstrap current flow in the opposite direction of the bootstrap current of the standard configuration with balanced helical currents.

In these studies we have calculated the 3D equilibria consistent with the bootstrap currents by applying the method developed by Watanabe et al.[5, 6]. The algorithm for calculation of the bootstrap current use a connection formula and is good from and including the $1/\nu$ regime to and including the Pfirsch-Schlüter regime. The plasma studied here is mostly in the region between the plateau and the $1/\nu$ regime.

The present paper is composed as follows: In Section 2, the method of calculation and the formula for the bootstrap currents are presented. The results of the calculation are shown and the mechanism for the change in direction of the bootstrap current is discussed in Section 3. In Section 4, the spatial axis effects on the MHD properties such as rotational transform, magnetic well and Mercier criterion are calculated. Conclusions are given in Section 5.

2 Calculation of Bootstrap Currents in LHD

To generate the vacuum spatial axis configurations for LHD, we have changed the ratio, I_1/I_2, of currents in the two helical coils from its standard configuration value of 1.0. For a given ratio, I_1/I_2, the magnitude of the currents is adjusted so as to keep strength of the magnetic field at the magnetic axis, B_0, equal to $2T$. In order to keep the averaged

magnetic axis at $R = 3.75$m, the position in the standard configuration, we have varied the total currents in the poloidal coils, but have kept their ratio fixed. As pointed out by Matsumoto et al.[12], we too found a tendency for the volume surrounded by the outermost good flux surface to shrink when the ratio I_1/I_2 gets farther from unity. In this case, the average radius is 0.576m for $I_1/I_2 = 100\%$ and 0.424m for $I_1/I_2 = 20\%$. We also note, that unbalancing the currents in the helical coils causes the number of field periods to change from 10 to 5.

By applying the method of Watanabe et al.[5, 6], we have calculated finite beta equilibria with self-consistent bootstrap currents. These finite beta calculations are fixed boundary calculations using the boundary of the vacuum solution described above. Our procedure is to first calculate the finite beta equilibrium by using the VMEC code[7] with the net toroidal current, $I(s)$, equal zero, where s is the toroidal magnetic flux normalized to unity at the outermost magnetic surface. Then using the magnetic fields found by VMEC, we calculate the bootstrap current, $I(s)$. This current is then input to the VMEC code and a new finite beta equilibrium is calculated. This procedure is iterated until convergence is achieved. In the evaluation of the bootstrap currents, we assumed that the plasma is composed of electrons and protons. The temperature, T, and the density, n, of the plasma are given by

$$T_e = T_i = T_0(1-s), \qquad n_e = n_i = n_0(1-s), \tag{2.1}$$

where subscripts 'e' and 'i' denote the values of electrons and ions, respectively.

The asymptotic expression for the bootstrap current has the same form in all collisionality regimes, the $1/\nu$, the plateau and the Pfirsch-Schlüter, and is given by

$$I_{BS}(s) = 2\pi \int ds \frac{\langle \boldsymbol{J}_{BS} \cdot \boldsymbol{B} \rangle}{\langle \boldsymbol{B}^2 \rangle}, \tag{2.2}$$

where

$$\langle \boldsymbol{J}_{BS} \cdot \boldsymbol{B} \rangle = -G_b \left[L_1 \frac{dP}{ds} + L_2 n \frac{dT}{ds} \right]. \tag{2.3}$$

Here P is the plasma pressure and L_1 and L_2 are the transport coefficients, which are composed of the viscosity and the collision coefficients. There is no contribution to the bootstrap current from the radial electric field because we are treating only the case where both temperature and density of the ion and electron are equal[13].

G_b is called a geometrical factor, since it depends on the geometry of the magnetic configuration. In axisymmetric configurations, such as tokamaks, G_b has the same form in all collisionality regimes and is given by

$$G_b^{tok} = J(s)/\iota, \tag{2.4}$$

where $2\pi J(s)$ means the total poloidal current outside of the magnetic surface labeled by s. On the other hand, in asymmetric configurations, such as LHD, the form of the expressions of G_b depends on the collisionality regime of the plasma. These forms have been derived only as asymptotic formulas in the three collisionality regimes, the $1/\nu$, the plateau and Pfirsch-Schlüter regimes. The asymptotic form for G_b in the $1/\nu$ regime, is given by following equations[13],

$$G_b^{1/\nu} = \frac{1}{f_t}\left\{\langle g_2\rangle - \frac{3}{4}\frac{\langle B^2\rangle}{B_{max}^2}\int_0^1 \frac{\langle g_4\rangle}{\langle g_1\rangle}\lambda d\lambda\right\}, \tag{2.5}$$

$$g_1 = \sqrt{1-\lambda\frac{B}{B_{max}}}, \tag{2.6}$$

where the bracket means the surface average and f_t is the fraction of the trapped particles given by

$$f_t = 1 - \frac{3}{4}\frac{\langle B^2\rangle}{B_{max}^2}\int_0^1 \frac{1}{\langle g_1\rangle}\lambda d\lambda. \tag{2.7}$$

g_2 and g_4 satisfy the magnetic differential equations of

$$\boldsymbol{B}\cdot\nabla\left(\frac{g_2}{B^2}\right) = \boldsymbol{B}\times\nabla\psi\cdot\nabla\left(\frac{1}{B^2}\right) \qquad g_2(B_{max}) = 0 \tag{2.8}$$

and

$$\boldsymbol{B}\cdot\nabla\left(\frac{g_4}{g_1}\right) = \boldsymbol{B}\times\nabla\psi\cdot\nabla\left(\frac{1}{g_1}\right), \qquad g_4(B_{max}) = 0, \tag{2.9}$$

respectively. The asymptotic form for G_b in the plateau regime is given by[6]

$$G_b^{pl} = \langle g_2\rangle - \frac{\sqrt{\pi}}{2}(J+\iota I)\lambda_{pl}\left\langle(\hat{\boldsymbol{n}}\cdot\nabla B)\sum_{m\neq 0\ or\ n\neq 0}\frac{1}{|m\iota+n|}\left(\frac{1}{2B^2}\hat{\boldsymbol{n}}\cdot\nabla g_2\right)_{mn}\exp i(m\theta+n\zeta)\right\rangle \tag{2.10}$$

$$\lambda_{pl} = \frac{2\langle B^2\rangle}{\sqrt{\pi}(J+\iota I)\left\langle(\hat{\boldsymbol{n}}\cdot\nabla B)\sum_{m\neq 0\ or\ n\neq 0}\frac{1}{|m\iota+n|}\left(\frac{1}{B}\hat{\boldsymbol{n}}\cdot\nabla B\right)_{mn}\exp i(m\theta+n\zeta)\right\rangle} \tag{2.11}$$

where

$$A_{mn} = \frac{1}{(2\pi)^2}\int_0^{2\pi} d\theta\int_0^{2\pi} d\zeta A\exp i(m\theta+n\zeta). \tag{2.12}$$

Here we employed the Boozer coordinates (s, θ, ζ)[14], where θ and ζ denote the poloidal and the toroidal angles, respectively. $\hat{\boldsymbol{n}}$ is the unit vector along the magnetic field, $\boldsymbol{B}$, and $2\pi I$ is the total toroidal current inside the flux surface. Since the plasma collisionality only varies from the $1/\nu$ to the plateau regimes in the present study, the geometrical factor in the Pfirsch-Schlüter regime is not discussed here.

In order to estimate the bootstrap current in the plasma with arbitrary collisionality, we employed connection formula derived by Watanabe et al.[6], with which the product of G_b and L_j (which also depends on collisionality) is interpolated from the asymptotic expressions. The normalized collision frequency, ν_* determines the collisionality of the particle and is given by

$$\nu_* = \frac{\nu}{\omega_b} = \frac{4}{3\sqrt{\pi}} \frac{f_t}{1 - f_t} \frac{\lambda_{pl}}{\lambda}, \tag{2.13}$$

where ν and ω_b denote the collision frequency and the bounce frequency of the banana motion of the particles, respectively. λ is the mean free path of the particle and λ_{pl} is the characteristic length of the magnetic field inhomogeneity. In the present case, the ν_*'s for electrons and ions are equal because they are assumed to have the same density and temperature. In terms of ν_* the plasma is in the $1/\nu$ regime if $\nu_* << 1$ and it is in the plateau regime if $\nu_* >> 1$, but less than the normalized transit frequency [6] . The product of G_b and L_j in arbitrary collisionality regime is given by a weighted combination of the product in each regime with the weight determined by ν_*.

3 Bootstrap Current in LHD with Spatial Axis Configurations

In our survey the temperature and the density of the plasma at the magnetic axis are fixed with $T_0 = 1.0keV$ and $n_0 = 0.5 \times 10^{20} m^{-3}$ in order to focus on the geometric effect of the unbalancing helical coil currents. Since the strength of the magnetic field at the magnetic axis, $B_0 = 2T$, the beta value at the magnetic axis, β_0, is 1.0% for all equilibrium studied here. The results of the procedure described in Chapter 2 are shown in Figures 1-3. Figure 1 shows the total bootstrap currents, $I_{BS}(s = 1)$, as a function of the ratio of the helical coil currents. In this figure, a positive value of the current corresponds to the

current flowing in a direction such as to increase the rotational transform. For example, in the standard configuration ($I_1/I_2 = 100\%$), the bootstrap current flows in the direction such as to increase the rotational transform. As the ratio of the helical coil currents decreases from 100% to 50%, the bootstrap current decreases only slightly. However, decreasing I_1/I_2 further causes a drastic decrease in the total bootstrap current. When $I_1/I_2 = 40\%$, the total current becomes almost zero and as I_1/I_2 continues to decrease the total current increases in the direction such as to decrease the rotational transform. Figure 2 shows the current density profiles given by expression (2.3). It is seen that the bootstrap current reverses from the magnetic axis to the edge as the ratio I_1/I_2 decreases.

Figure 3 shows the profiles of the geometrical factors $G_b^{1/\nu}$ and G_b^{pl} for equilibria with $I_1/I_2 = 100$, 70, 40 and 20 %. Both $G_b^{1/\nu}$ and G_b^{pl} are normalized by G_b^{tok}. $G_b^{1/\nu}$ changes drastically from positive to negative as the ratio of the helical coil currents decreases, while G_b^{pl} is fairly constant. The profiles of the current density in Fig.2 are, thus, mainly due to the changes in $G_b^{1/\nu}$. The transport coefficient L_j also depends on the magnetic structure, however, L_j is fairly insensitive to the ratio I_1/I_2 and we thus discuss only the dependency of G_b rather than the product of G_b and L_j.

The reason $G_b^{1/\nu}$ dominates is seen in Fig.4, where we plotted the normalized collision frequency ν_*. Over most of the plasma column, ν_* is less than unity for all values of I_1/I_2. Furthermore, ν_* decreases below unity in the vicinity of the magnetic axis as I_1/I_2 decreases. Thus, it is clear why the contribution of $G_b^{1/\nu}$ is larger than that of G_b^{pl} in the connection formula.

Now we investigate how the change of the magnetic structure affects $G_b^{1/\nu}$ when I_1/I_2 is decreased. For this purpose, we decomposed the strength of the magnetic field into the spectrums, B_{mn}, as

$$B = \sum_{m,n} B_{mn}(s)\cos(m\theta + n\zeta), \tag{3.1}$$

where m and n denote the poloidal and the toroidal Fourier mode numbers in the Boozer coordinates, respectively. Figure 5 shows the largest six modes in the cases where $I_1/I_2 = 70\%$ and 20%, which correspond to positive and the negative bootstrap currents, respectively. In the case of $I_1/I_2 = 70\%$, the components of $B_{2,10}$ and $B_{1,0}$ are dominant. These are the basic components in the standard configuration with a planar axis in LHD, and effect the ellipticity of the flux surface and the toroidicity of the system. In the case $I_1/I_2 = 20\%$,

$B_{1,5}$ and $B_{0,5}$ dominate the spectrum. $B_{1,5}$ is related to the creation of the spatial axis and $B_{0,5}$ is related to the bumpiness of the magnetic field. In order to illustrate that $B_{1,5}$ and $B_{0,5}$ are the dominant harmonics in the magnetic spectrum determining $G_b^{1/\nu}$, we plot in Fig.6, profiles of $G_b^{1/\nu}$, omitting no modes, omitting the contribution of $B_{0,5}$, omitting the contribution of $B_{1,5}$, and omitting the contribution of both $B_{0,5}$ and $B_{1,5}$. When we omit both components, the profile of $G_b^{1/\nu}$ becomes positive and the absolute value is comparable with the one including the all modes. As is shown in the case where $B_{1,5}$ or $B_{0,5}$ is omitted, it is impossible to make the sign of $G_b^{1/\nu}$ negative with only one mode of them. Therefore, not only the spatial axis component but also the bumpiness component in the magnetic field contribute to the change of the direction of the bootstrap current.

Next we discuss the reason for the decrease of ν_* in the vicinity of the magnetic axis seen in Fig.4. This decrease is due to the increase in the bumpiness of the magnetic field. Since $B_{m\neq 0,n}$ approaches zero as $s \to 0$, only the components of B_{0n} survive near the magnetic axis in the denominator of λ_{pl} given by equation (2.13). For $I_1/I_2 = 70\%$, the components with $m = 0$ are small, e.g., $B_{0,5}$ is only 3% of B_{00}. However, when $I_1/I_2 = 20\%$, $B_{0,5}$ is about 15% of B_{00} and therefore, λ_{pl} for this case is smaller than in the case $I_1/I_2 = 70\%$. The reduction of λ_{pl} by B_{0n} implies the enhancement of ω_b due to the magnetic mirror generated by the bumpiness. The bumpiness of the field also causes the fraction of trapped particles, f_t, to increase and as seen from equation (2.13) this leads to an increase in ν_* . However, the reduction of λ_{pl} is more important and ν_* decreases.

4 MHD Properties in Spatial Axis Equilibria with Bootstrap Currents

Here we consider how the MHD properties, such as rotational transform, magnetic well, and Mercier stability change when the equilibrium developes a spatial axis in the presence of bootstrap current. In contrast to the studies of Matsumoto et al.[12] on currentless spatial axis effects, we find that when the bootstrap current effect is also included, some of the MHD properties change substantially.

The rotational transform of the equilibria used in this study are presented in Fig.7.

There are three effects that contribute to the change in the rotational transform for these equilibria. The first is the modification of the vacuum field due to the unbalanced helical currents. This is illustrated in Fig.7 (a). The radial coordinate in these plots, as well as the following plots, is the average radius. We use the average radius since, as mentioned in Chapter 2, the plasma column shrinks as I_1/I_2 decreases. Thus, using the average radius compares quantities at roughly the same spatial location. We observe a general increase in the rotational transform as I_1/I_2 decreases. This increase is due to the increase in the torsion of the magnetic axis[15].

When finite beta is added to the equilibria, two other effects contribute to the changing rotational transform profile. One is the modification of the poloidal flux caused by the bootstrap currents. The other is due to the Shafranov shift[16] caused by the finite beta. These effects are shown in Fig.7 (b). The former effect influences the latter because the reduction of the rotational transform by the net toroidal current enhances the Shafranov shift[8]. Thus, it is observed that there is a major modification of the transform at $I_1/I_2 = 20\%$ attributed to the latter effect. In this case, the profile changes so as to have a minimum value in the plasma column, and large shear is introduced in the peripheral region. This enhanced shear has a significantly effect on Mercier stability, which we discussed below.

Configurations with small ratios of I_1/I_2 also enhance the magnetic well as shown in Fig.8. Here the magnetic well depth defined by $(V'(0) - V'(s))/V'(0)$ is plotted, where V is the volume of the flux tube and the prime means the derivative with respect to s. A positive gradient of the well depth corresponds to a magnetic well ($V'' < 0$). When the bootstrap current flows in the direction to decrease the rotational transform ($I_1/I_2 < 40\%$), the region of the magnetic well is extended and is deepened. A deep magnetic well region covers almost half region of the plasma column in the case $I_1/I_2 = 20\%$. (The outer half has an unfavorable hill, but this is also reduced from the case $I_1/I_2 = 100\%$.) Such a magnetic well is favorable for stability against the interchange mode. In order to show that the appearance of this well is due to the bootstrap current, we have rerun these cases under the zero net current constraint. The results for these currentless equilibria show that there is little difference in the well depth structure among them. The equilibria carrying the bootstrap current have larger well depth than the currentless value for $I_1/I_2 = 20\%$ and 40% and smaller one for $I_1/I_2 = 70\%$ and 100%. This confirms the conjecture that

the improved well depth obtained here is due to the bootstrap current, while Matsumoto et al.[12] have found the improvement attributed to the shrinkage of the plasma column in the currentless case with $\beta_0 = 10\%$.

Shown in Fig.9 is the Mercier criterion. Here D_I, is normalized so that the shear term in the criterion is 1/4[8] and $D_I > 0$ implies instability. It is seen that equilibria with $I_1/I_2 \leq 40\%$ are completely stable against the interchange mode. This result is due to the stabilizing effect of the increased magnetic shear and the deep magnetic well brought about by the bootstrap current flowing in a direction that decreases the rotational transform. Again, to verify that the effect is due to the bootstrap current, we have repeated these runs for currentless equilibria and have found them to be Mercier unstable.

5 Conclusion

We have studied bootstrap current in LHD configurations with unbalanced currents flowing in the helical coils. We calculated the self-consistent bootstrap currents with 3D equilibria, with $n_e = n_i = 0.5 \times 10^{20}(1-s)(\mathrm{m}^{-3})$ and $T_e = T_i = 1.0 \times (1-s)(\mathrm{keV})$. A connection formula for the products of the geometrical factor and the transport coefficient is employed in order to evaluate the bootstrap current for the collisionality determined by the given parameters. In the standard configuration, the bootstrap current flows in the direction such as to increase the rotational transform. As I_1/I_2 decreases, the bootstrap current decreases and after that, reverses direction. It is shown that this change of the bootstrap current is dominantly determined by the behavior of $G_b^{1/\nu}$. This can be understood from the fact that $G_b^{1/\nu}$ has dominant contribution in the connection formula because ν_* in the plasma used here is less than unity.

It is found that the enhancement of the $\ell = 1$ component, $B_{1,5}$, and the bumpiness component of the magnetic field, $B_{0,5}$, are essential to insure that $G_b^{1/\nu}$ has a negative value. This leads to the reversal in the bootstrap current. The importance of the $B_{1,5}$ was suggested by Shaing et al.[11]. Here we find that the $B_{0,5}$ component also is major contributor to the change of $G_b^{1/\nu}$. Furthermore, bumpiness of the magnetic field increases the bounce frequency of the banana motion. This results in the reduction of ν_* and this

leads to a large contribution of $G_b^{1/\nu}$ in the connection formula. In the helias configurations, the bumpiness of the magnetic field has also been recognized as one of the important parameters in the optimization with respect to the bootstrap current[17].

The bootstrap currents strongly affect the MHD properties. When $I_1/I_2 < 40\%$ so that the bootstrap current flows in the direction such as to decrease the rotational transform, we observe the increase in the shear and magnetic well depth. Therefore, the Mercier mode can be stabilized by unbalancing the helical coil currents through the effects of the bootstrap current. These properties are quite different from those in the currentless equilibria studied by Matsumoto et al.[12], in which case the dominant effects on the MHD properties are the change of the aspect ratio and rather than spatial axis effects.

Acknowledgments

One of the authors (K.I.) would like to thank Dr.D.Monticello for his many fruitful discussions.

References

[1] IIYOSHI,A., FUJIWARA,M., MOTOJIMA,O., OYABU,N., YAMAZAKI,K., Fusion Tech. **17** (1990) 169.

[2] IIYOSHI,A., YAMAZAKI,K., Phys. Plasmas **2** (1995) 2349.

[3] NAKAJIMA,N., OKAMOTO,M., TODOROKI,J., NAKAMURA,Y., WAKATANI,M., Nucl. Fusion **29** (1989) 605.

[4] NAKAJIMA,N., OKAMOTO,M., J. Phys. Soc. Jpn. **61** (1992) 833.

[5] WATANABE,K., NAKAJIMA,N., OKAMOTO,M., NAKAMURA,Y., WAKATANI,M., Nucl. Fusion **32** (1992) 1499.

[6] WATANABE,K.Y., NAKAJIMA,N., OKAMOTO,M., YAMAZAKI,K., NAKAMURA,Y., WAKATANI,M., Nucl. Fusion **35** (1995) 335.

[7] HIRSHMAN,S.P., VAN RIJ,W.I., MERKEL,P., Comp. Phys. Comm. **43** (1986) 143.

[8] ICHIGUCHI,K., NAKAJIMA,N., OKAMOTO,M., NAKAMURA,Y., WAKATANI,M., Nucl. Fusion **33** (1993) 481.

[9] MERCIER,C., Nucl. Fusion Suppl. Pt.2, (1962) 801.

[10] JOHNSON,J.L., GREENE,J.M., Plasma Phys. **9** (1967) 611.

[11] SHAING,K.C., CARRERAS,B.A., DOMINGUEZ, N., LYNCH, V.E., TOLLIVER, J.S., Phys. Fluids **B1** (1989) 1663.

[12] MATSUMOTO,T., NAKAMURA,Y., WAKATANI,M., J. Phys. Soc. Jpn. **64** (1995) 4175.

[13] NAKAJIMA,N., OKAMOTO,M., FUJIWARA,M., Kakuyugo Kenkyu, **68** (1992) 503.

[14] BOOZER, A.H., Phys. Fluids **25** (1982) 520.

[15] ICHIGUCHI,K., WAKATANI,M., Nucl. Fusion **28** (1988) 411.

[16] MATVEEVA.E.A., PUSTOVITOV,V.D., JETP Lett. **45** (1987) 268.

[17] MAASSBERG,H., LOTZ,W., NÜHRENBERG,J., Phys. Fluids **B5** (1993) 3728.

Figure Captions

Fig.1 Total net toroidal currents versus I_1/I_2. Positive values correspond to the direction of increasing rotational transform and negative values correspond to the direction of decreasing rotational transform.

Fig.2 Profiles of the toroidal current density, $\langle \boldsymbol{J}\cdot\boldsymbol{B}\rangle/\langle \boldsymbol{B}^2\rangle$ in arbitrary unit for I_1/I_2 =100, 70, 40 and 20%.

Fig.3 Profiles of geometrical factors in (a) $1/\nu$ regime and (b) plateau regime for I_1/I_2 =100, 70, 40 and 20%.

Fig.4 Profiles of the effective collision frequency for I_1/I_2 =100, 70, 40, 20%.

Fig.5 Spectrum of the magnetic field for (a) I_1/I_2=70% and (a) I_1/I_2=20% in the Boozer coordinates. Each mode is normalized by $B_{00}(s=0)$. $[B_{00}(s)-B_{00}(s=0)]/B_{00}(s=0)$ is plotted for $(m,n)=(0,0)$.

Fig.6 Profiles of geometrical factor in $1/\nu$ regime for I_1/I_2 =20%, omitting no modes (solid line), omitting only the $B_{0,5}$ component (dashed line), omitting only the $B_{1,5}$ component (dot-dashed line) and omitting both the $B_{0,5}$ and the $B_{1,5}$ components (two-dot-dashed line).

Fig.7 Rotational transform profiles at β_0 = (a) 0% and (b) 1% for I_1/I_2 =100, 70, 40 and 20%.

Fig.8 Magnetic well depth at $\beta_0 = 1\%$ for I_1/I_2 =100, 70, 40 and 20%.

Fig.9 Mercier criterion D_I at $\beta_0 = 1\%$ for I_1/I_2 =100, 70, 40 and 20%.

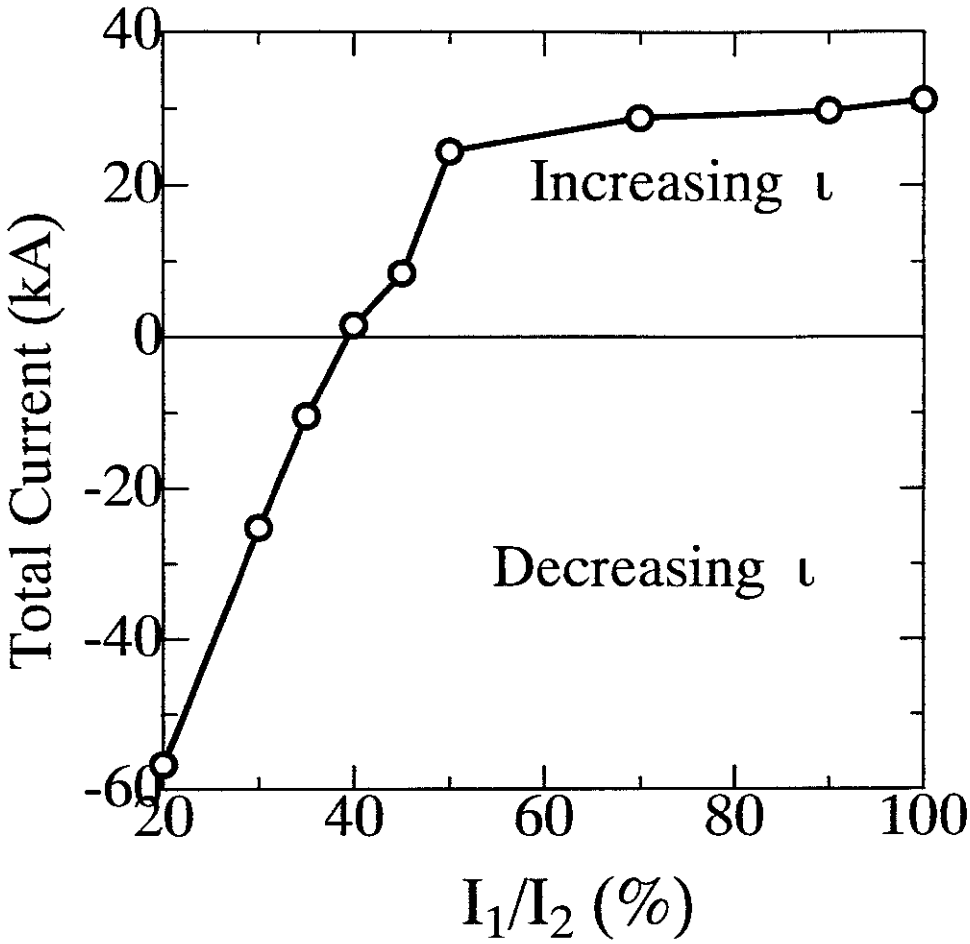
40
20
0
-20
-40
-60
Total Current (kA)
Increasing ι
Decreasing ι
20
40
60
80
100
I1/I2 (%)

Fig.1

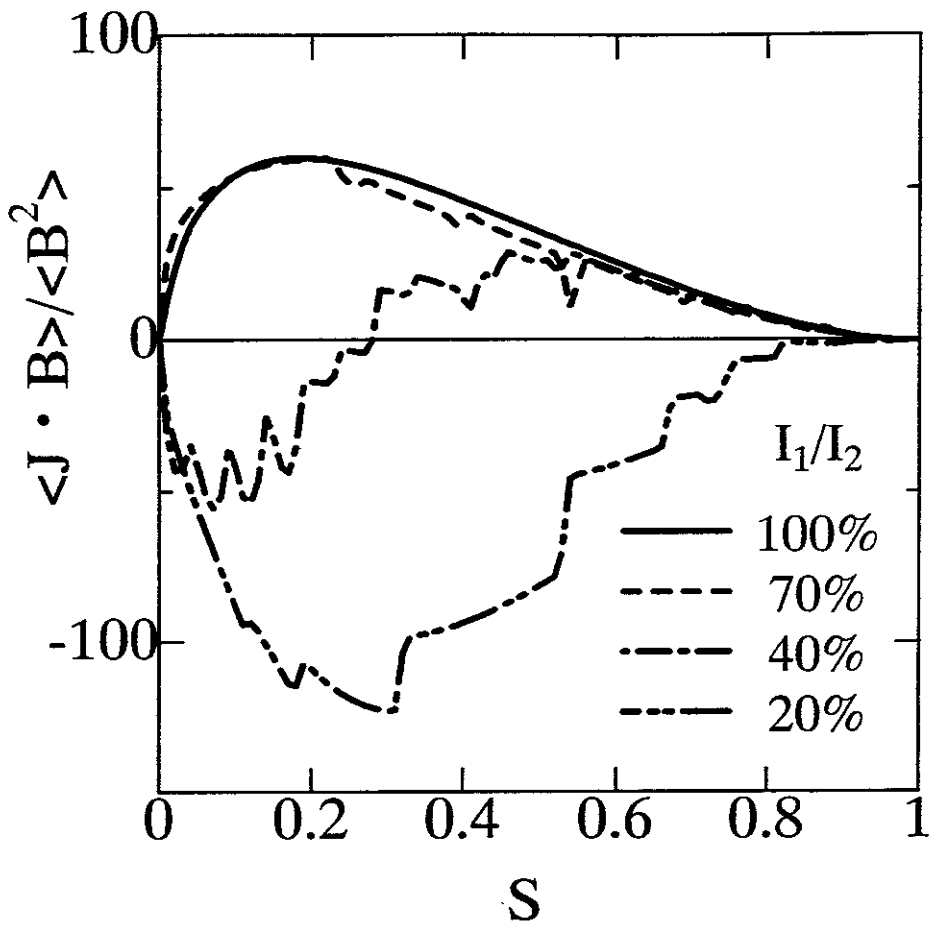

Fig.2

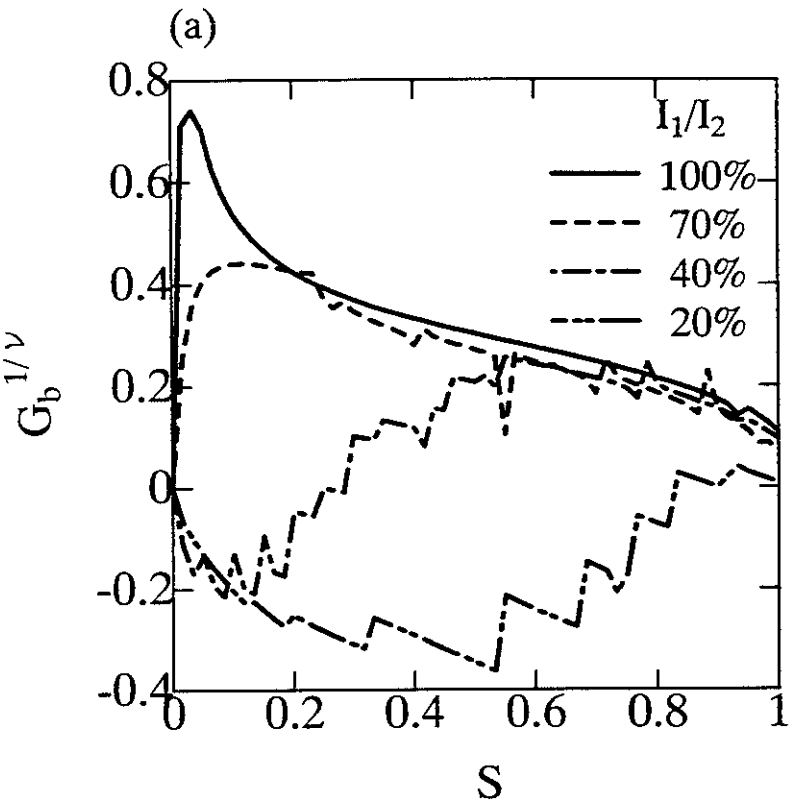
(a)
0.8
0.6
0.4
0.2
0
-0.2
-0.4
0
0.2
0.4
0.6
0.8
1
S
$G_b^{1/\nu}$
I_1/I_2
100%
70%
40%
20%

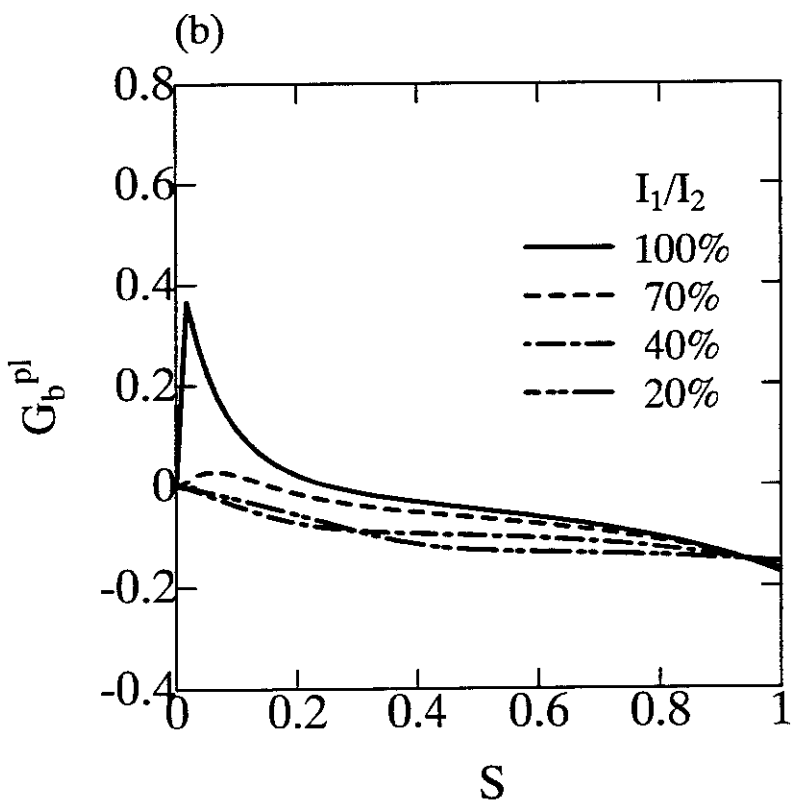
(b)
0.8
0.6
0.4
0.2
0
-0.2
-0.4
0
0.2
0.4
0.6
0.8
1
S
G_b^{pl}
I_1/I_2
100%
70%
40%
20%

Fig.3

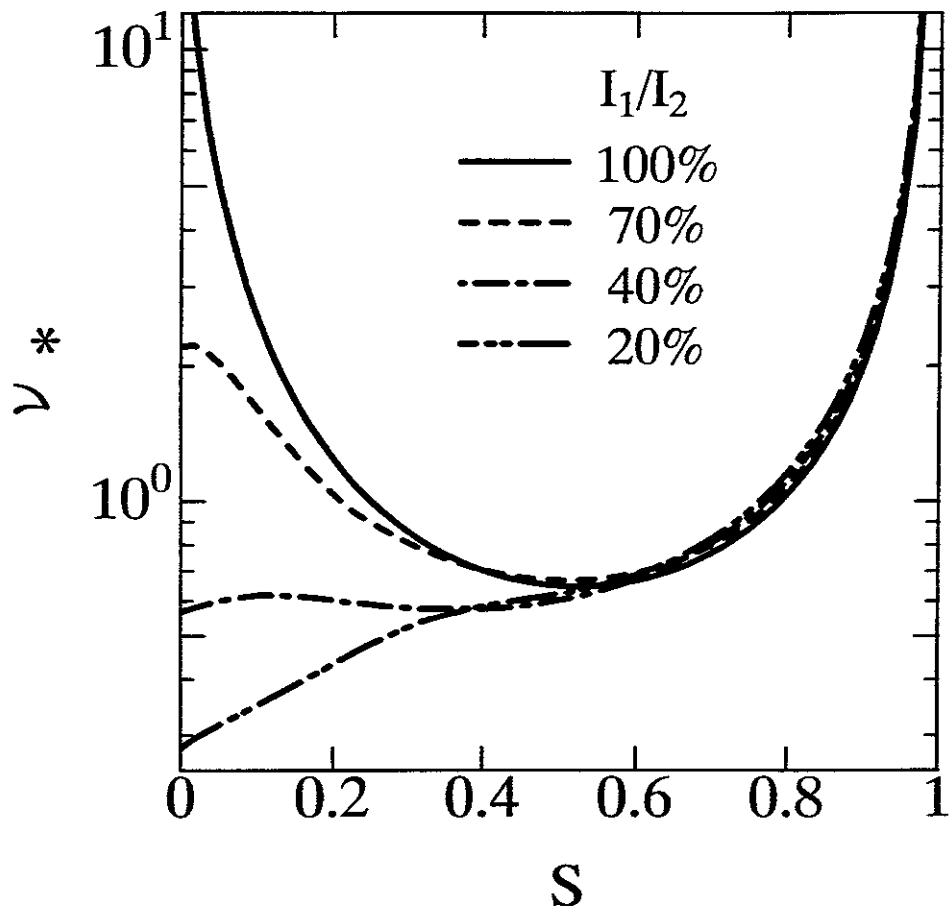

Fig.4

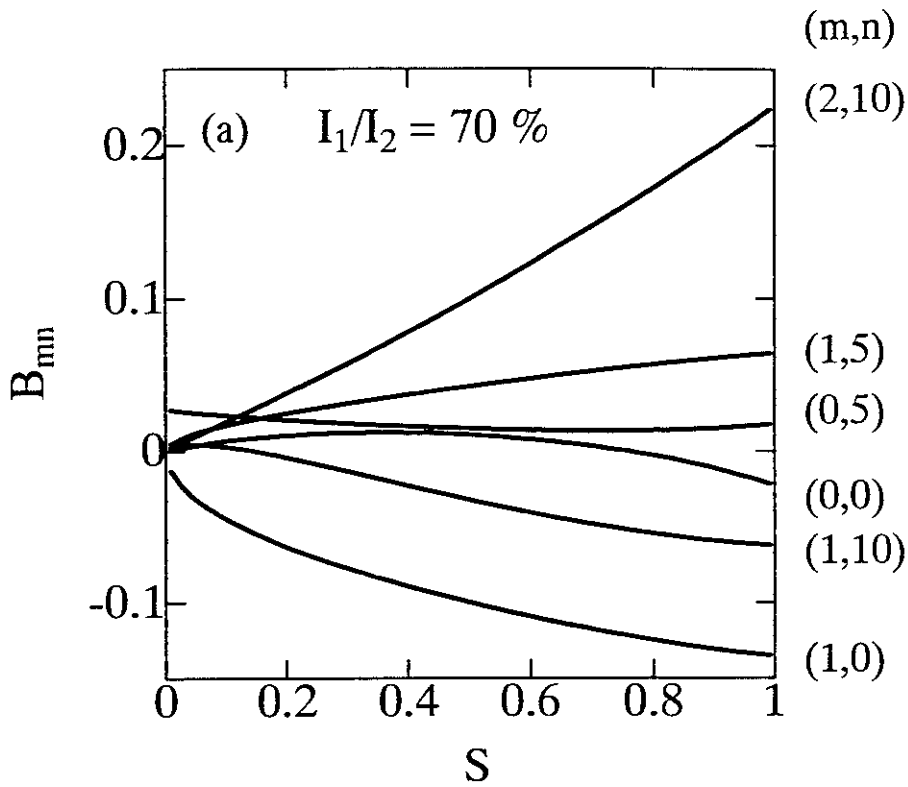
(m,n)
(a) I_1/I_2 = 70 %
(2,10)
(1,5)
(0,5)
(0,0)
(1,10)
(1,0)
B_{mn}
0.2
0.1
0
-0.1
0
0.2
0.4
0.6
0.8
1
S

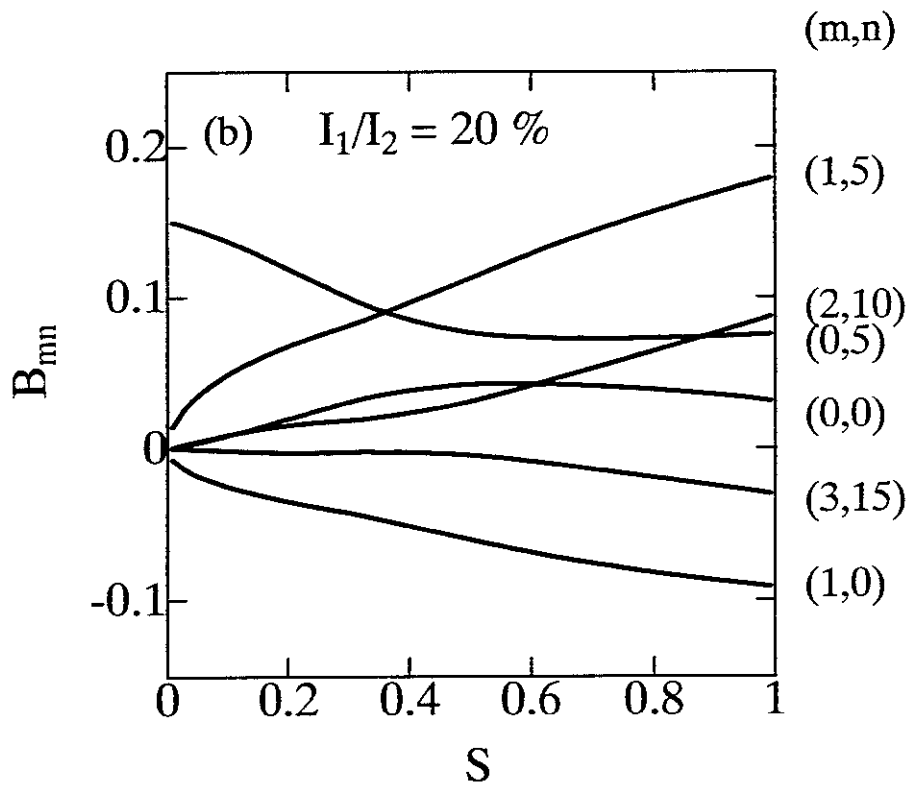
(m,n)
(b) I_1/I_2 = 20 %
(1,5)
(2,10)
(0,5)
(0,0)
(3,15)
(1,0)
B_{mn}
0.2
0.1
0
-0.1
0
0.2
0.4
0.6
0.8
1
S

Fig.5

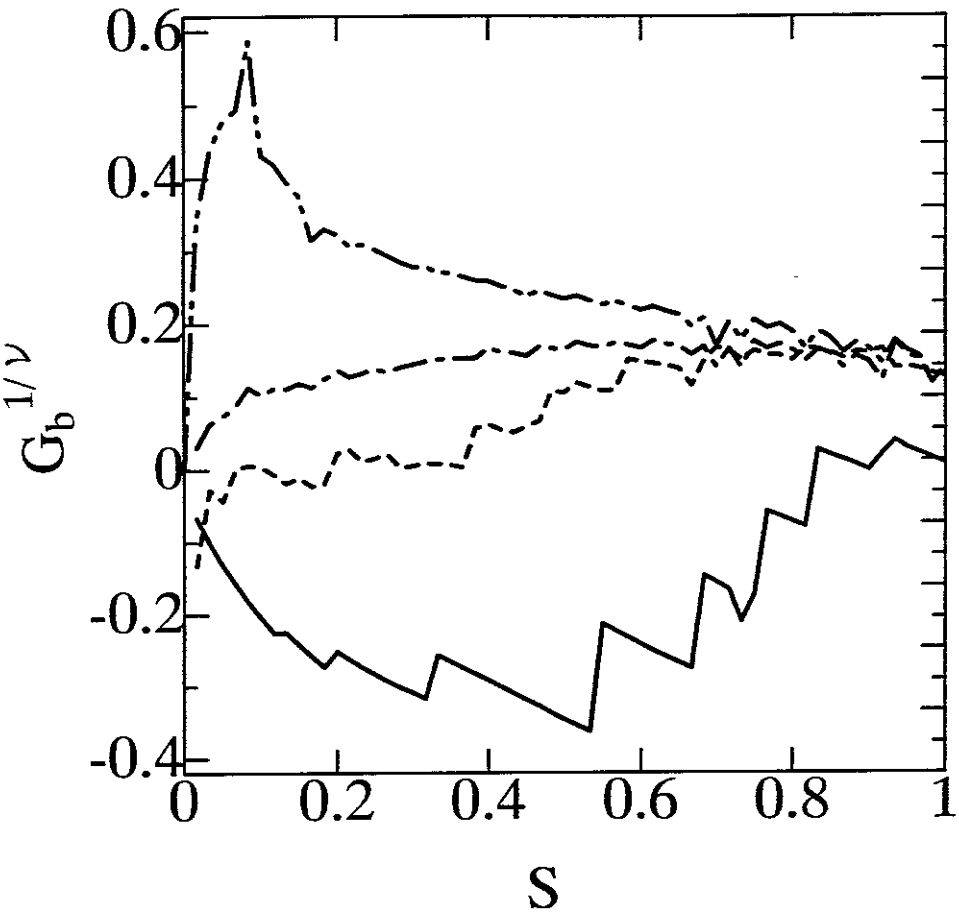

Fig.6

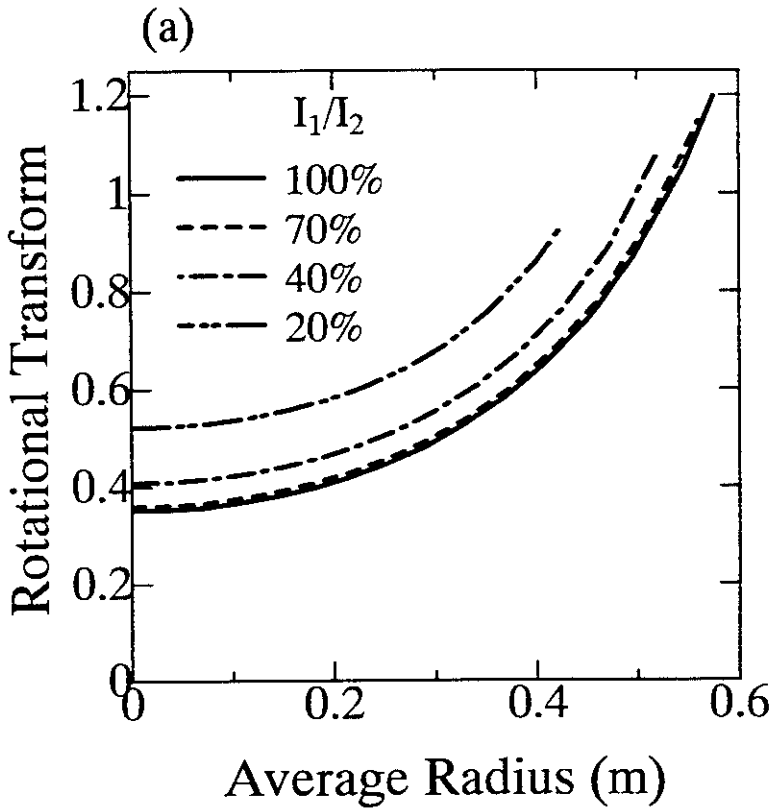
(a)
Rotational Transform
Average Radius (m)
I_1/I_2
100%
70%
40%
20%
0
0.2
0.4
0.6
0.8
1
1.2
0
0.2
0.4
0.6

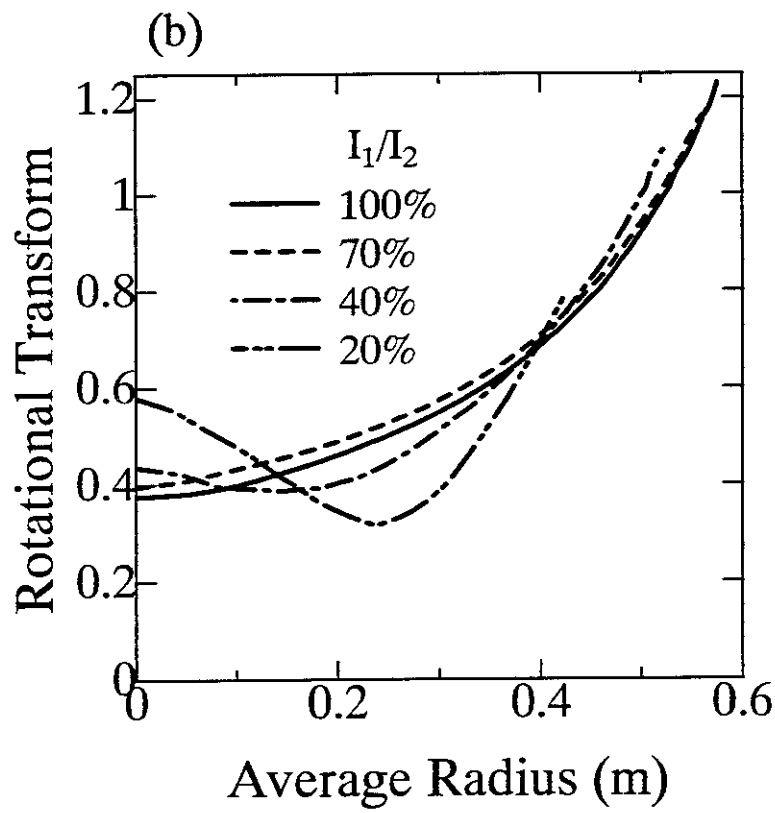
(b)
Rotational Transform
Average Radius (m)
I_1/I_2
100%
70%
40%
20%
0
0.2
0.4
0.6
0.8
1
1.2
0
0.2
0.4
0.6

Fig.7

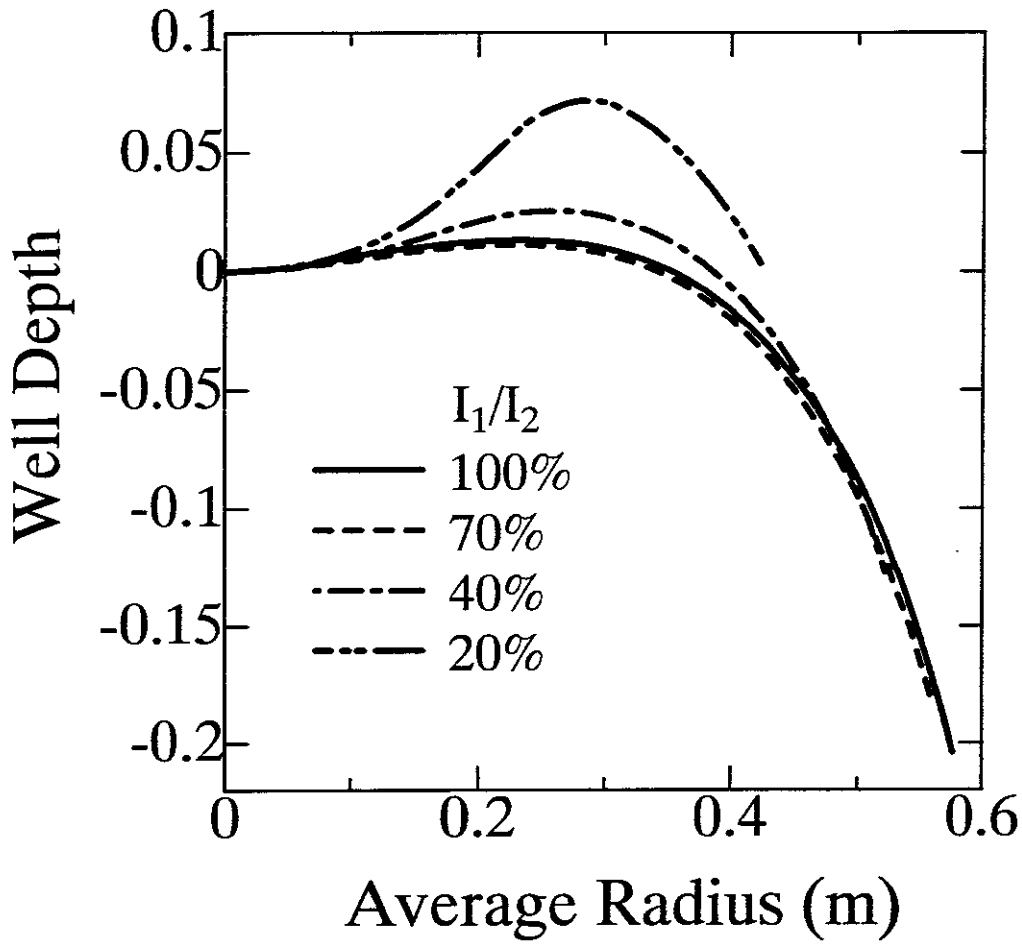
0.1
0.05
0
-0.05
-0.1
-0.15
-0.2
Well Depth
0
0.2
0.4
0.6
Average Radius (m)
I1/I2
100%
70%
40%
20%

Fig.8

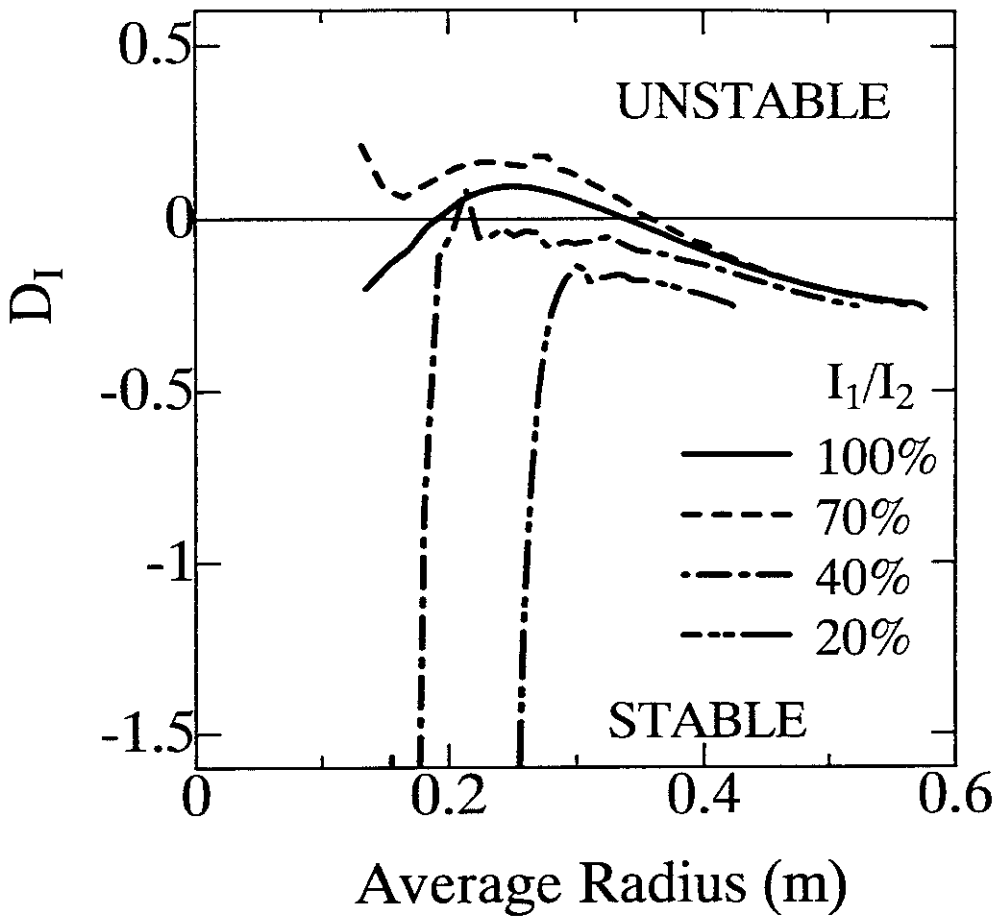
0.5
0
-0.5
-1
-1.5
D_I
UNSTABLE
STABLE
I_1/I_2
100%
70%
40%
20%
0
0.2
0.4
0.6
Average Radius (m)

Fig.9

Recent Issues of NIFS Series

NIFS-447 K. Yamazaki, A. Sagara, O. Motojima, M. Fujiwara, T. Amano, H. Chikaraishi, S. Imagawa, T. Muroga, N. Noda, N. Ohyabu, T. Satow, J.F. Wang, K.Y. Watanabe, J. Yamamoto , H. Yamanishi, A. Kohyama, H. Matsui, O. Mitarai, T. Noda, A.A. Shishkin, S. Tanaka and T. Terai
Design Assessment of Heliotron Reactor; Sep. 1996 (IAEA-CN-64/G1-5)

NIFS-448 M. Ozaki, T. Sato and the Complexity Simulation Group,
Interactions of Convecting Magnetic Loops and Arcades; Sep. 1996

NIFS-449 T. Aoki,
Interpolated Differential Operator (IDO) Scheme for Solving Partial Differential Equations; Sep. 1996

NIFS-450 D. Biskamp and T. Sato,
Partial Reconnection in the Sawtooth Collapse; Sep. 1996

NIFS-451 J. Li, X. Gong, L. Luo, F.X. Yin, N. Noda, B. Wan, W. Xu, X. Gao, F. Yin, J.G. Jiang, Z. Wu., J.Y. Zhao, M. Wu, S. Liu and Y. Han,
Effects of High Z Probe on Plasma Behavior in HT-6M Tokamak; Sep. 1996

NIFS-452 N. Nakajima, K. Ichiguchi, M. Okamoto and R.L. Dewar,
Ballooning Modes in Heliotrons/Torsatrons; Sep. 1996 (IAEA-CN-64/D3-6)

NIFS-453 A. Iiyoshi,
Overview of Helical Systems; Sep. 1996 (IAEA-CN-64/O1-7)

NIFS-454 S. Saito, Y. Nomura, K. Hirose and Y.H. Ichikawa,
Separatrix Reconnection and Periodic Orbit Annihilation in the Harper Map; Oct. 1996

NIFS-455 K. Ichiguchi, N. Nakajima and M. Okamoto,
Topics on MHD Equilibrium and Stability in Heliotron / Torsatron; Oct. 1996

NIFS-456 G. Kawahara, S. Kida, M. Tanaka and S. Yanase,
Wrap, Tilt and Stretch of Vorticity Lines around a Strong Straight Vortex Tube in a Simple Shear Flow; Oct. 1996

NIFS-457 K. Itoh, S.- I. Itoh, A. Fukuyama and M. Yagi,
Turbulent Transport and Structural Transition in Confined Plasmas; Oct. 1996

NIFS-458 A. Kageyama and T. Sato,
Generation Mechanism of a Dipole Field by a Magnetohydrodynamic Dynamo; Oct. 1996

NIFS-459 K. Araki, J. Mizushima and S. Yanase,
The Non-axisymmetric Instability of the Wide-Gap Spherical Couette Flow; Oct. 1996

NIFS-460 Y. Hamada, A. Fujisawa, H. Iguchi, A. Nishizawa and Y. Kawasumi,
A Tandem Parallel Plate Analyzer; Nov. 1996

NIFS-461 Y. Hamada, A. Nishizawa, Y. Kawasumi, A. Fujisawa, K. Narihara, K. Ida, A. Ejiri, S. Ohdachi, K. Kawahata, K. Toi, K. Sato, T. Seki, H. Iguchi, K. Adachi, S. Hidekuma, S.Hirokura, K. Iwasaki, T. Ido, M. Kojima, J. Koong, R. Kumazawa, H. Kuramoto, T. Minami, I. Nomura, H. Sakakita, M. Sasao, K.N. Sato, T. Tsuzuki, J. Xu, I. Yamada and T. Watari,
Density Fluctuation in JIPP T-IIU Tokamak Plasmas Measured by a Heavy Ion Beam Probe; Nov. 1996

NIFS-462 N. Katsuragawa, H. Hojo and A. Mase,
Simulation Study on Cross Polarization Scattering of Ultrashort-Pulse Electromagnetic Waves; Nov. 1996

NIFS-463 V. Voitsenya, V. Konovalov, O. Motojima, K. Narihara, M. Becker and B. Schunke,
Evaluations of Different Metals for Manufacturing Mirrors of Thomson Scattering System for the LHD Divertor Plasma; Nov. 1996

NIFS-464 M. Pereyaslavets, M. Sato, T. Shimozuma, Y. Takita, H. Idei, S. Kubo, K. Ohkubo and K. Hayashi,
Development and Simulation of RF Components for High Power Millimeter Wave Gyrotrons; Nov. 1996

NIFS-465 V.S. Voitsenya, S. Masuzaki, O. Motojima, N. Noda and N. Ohyabu,
On the Use of CX Atom Analyzer for Study Characteristics of Ion Component in a LHD Divertor Plasma; Dec. 1996

NIFS-466 H. Miura and S. Kida,
Identification of Tubular Vortices in Complex Flows; Dec. 1996

NIFS-467 Y. Takeiri, Y. Oka, M. Osakabe, K. Tsumori, O. Kaneko, T. Takanashi, E. Asano, T. Kawamoto, R. Akiyama and T. Kuroda,
Suppression of Accelerated Electrons in a High-current Large Negative Ion Source; Dec. 1996

NIFS-468 A. Sagara, Y. Hasegawa, K. Tsuzuki, N. Inoue, H. Suzuki, T. Morisaki, N. Noda, O. Motojima, S. Okamura, K. Matsuoka, R. Akiyama, K. Ida, H. Idei, K. Iwasaki, S. Kubo, T. Minami, S. Morita, K. Narihara, T. Ozaki, K. Sato, C. Takahashi, K. Tanaka, K. Toi and I. Yamada,
Real Time Boronization Experiments in CHS and Scaling for LHD; Dec. 1996

NIFS-469 V.L. Vdovin, T.Watari and A. Fukuyama,
3D Maxwell-Vlasov Boundary Value Problem Solution in Stellarator Geometry in Ion Cyclotron Frequency Range (final report); Dec. 1996

NIFS-470 N. Nakajima. M. Yokoyama. M. Okamoto and J. Nührenberg,
Optimization of M=2 Stellarator; Dec. 1996

NIFS-471 A. Fujisawa. H. Iguchi, S. Lee and Y. Hamada,
Effects of Horizontal Injection Angle Displacements on Energy Measurements with Parallel Plate Energy Analyzer; Dec. 1996

NIFS-472 R. Kanno, N. Nakajima, H. Sugama, M. Okamoto and Y. Ogawa,
Effects of Finite-β and Radial Electric Fields on Neoclassical Transport in the Large Helical Device; Jan. 1997

NIFS-473 S. Murakami, N. Nakajima, U. Gasparino and M. Okamoto,
Simulation Study of Radial Electric Field in CHS and LHD; Jan. 1997

NIFS-474 K. Ohkubo, S. Kubo, H. Idei, M. Sato, T. Shimozuma and Y. Takita,
Coupling of Tilting Gaussian Beam with Hybrid Mode in the Corrugated Waveguide; Jan. 1997

NIFS-475 A. Fujisawa, H. Iguchi, S. Lee and Y. Hamada,
Consideration of Fluctuation in Secondary Beam Intensity of Heavy Ion Beam Prove Measurements; Jan. 1997

NIFS-476 Y. Takeiri, M. Osakabe, Y. Oka, K. Tsumori, O. Kaneko, T. Takanashi, E. Asano, T. Kawamoto, R. Akiyama and T. Kuroda,
Long-pulse Operation of a Cesium-Seeded High-Current Large Negative Ion Source; Jan. 1997

NIFS-477 H. Kuramoto, K. Toi, N. Haraki, K. Sato, J. Xu, A. Ejiri, K. Narihara, T. Seki, S. Ohdachi, K. Adati, R. Akiyama, Y. Hamada, S. Hirokura, K. Kawahata and M. Kojima,
Study of Toroidal Current Penetration during Current Ramp in JIPP T-IIU with Fast Response Zeeman Polarimeter; Jan., 1997

NIFS-478 H. Sugama and W. Horton,
Neoclassical Electron and Ion Transport in Toroidally Rotating Plasmas; Jan. 1997

NIFS-479 V.L. Vdovin and I.V. Kamenskij,
3D Electromagnetic Theory of ICRF Multi Port Multi Loop Antenna; Jan. 1997

NIFS-480 W.X. Wang, M. Okamoto, N. Nakajima, S Murakami and N. Ohyabu,
Cooling Effect of Secondary Electrons in the High Temperature Divertor Operation; Feb. 1997

NIFS-481 K. Itoh, S.-I. Itoh, H. Soltwisch and H.R. Koslowski,
Generation of Toroidal Current Sheet at Sawtooth Crash; Feb. 1997

NIFS-482 K. Ichiguchi,

Collisionality Dependence of Mercier Stability in LHD Equilibria with Bootstrap Currents; Feb. 1997

NIFS-483 S. Fujiwara and T. Sato,
Molecular Dynamics Simulations of Structural Formation of a Single Polymer Chain: Bond-orientational Order and Conformational Defects; Feb. 1997

NIFS-484 T. Ohkawa,
Reduction of Turbulence by Sheared Toroidal Flow on a Flux Surface; Feb. 1997

NIFS-485 K. Narihara, K. Toi, Y. Hamada, K. Yamauchi, K. Adachi, I. Yamada, K. N. Sato, K. Kawahata, A. Nishizawa, S. Ohdachi, K. Sato, T. Seki, T. Watari, J. Xu, A. Ejiri, S. Hirokura, K. Ida, Y. Kawasumi, M. Kojima, H. Sakakita, T. Ido, K. Kitachi, J. Koog and H. Kuramoto,
Observation of Dusts by Laser Scattering Method in theJIPPT-IIU Tokamak Mar. 1997

NIFS-486 S. Bazdenkov, T. Sato and The Complexity Simulation Group,
Topological Transformations in Isolated Straight Magnetic Flux Tube; Mar. 1997

NIFS-487 M. Okamoto,
Configuration Studies of LHD Plasmas; Mar. 1997

NIFS-488 A. Fujisawa, H. Iguchi, H. Sanuki, K. Itoh, S. Lee, Y. Hamada, S. Kubo, H. Idei, R. Akiyama, K. Tanaka, T. Minami, K. Ida, S. Nishimura, S. Morita, M. Kojima, S. Hidekuma, S.-I. Itoh, C. Takahashi, N. Inoue, H. Suzuki, S. Okamura and K. Matsuoka,
Dynamic Behavior of Potential in the Plasma Core of the CHS Heliotron/Torsatron; Apr. 1997

NIFS-489 T. Ohkawa,
Pfirsch - Schlüter Diffusion with Anisotropic and Nonuniform Superthermal Ion Pressure; Apr. 1997

NIFS-490 S. Ishiguro and The Complexity Simulation Group,
Formation of Wave-front Pattern Accompanied by Current-driven Electrostatic Ion-cyclotron Instabilities; Apr. 1997

NIFS-491 A. Ejiri, K. Shinohara and K. Kawahata,
An Algorithm to Remove Fringe Jumps and its Application to Microwave Reflectometry; Apr. 1997

NIFS-492 K. Ichiguchi, N. Nakajima, M. Okamoto,
Bootstrap Current in the Large Helical Device with Unbalanced Helical Coil Currents; Apr. 1997